

Ion-Regulated Interfacial Rheology and Dynamic Recovery Mechanisms of Low-Salinity Waterflooding[#]

Yuting HE¹, Yuetian LIU^{1*}, Rukuan CHAI², Ying MENG^{3*}

1 State Key Laboratory of Petroleum Resources and Engineering, China University of Petroleum (Beijing), Beijing, China

2 Imperial College London, SW7 2AZ London, United Kingdom

3 School of Mathematics and Systems Science, Shenyang Normal University, Shenyang 110034, China

(Corresponding Author: lyt51@163.com)

ABSTRACT

This study investigates the effect of low-salinity waterflooding on enhanced oil recovery, focusing on how different cation types (Na^+ , Ca^{2+} , Mg^{2+}) and their concentrations influence the interfacial structure and viscoelastic properties of stearic acid monolayers at the oil-water interface. The results demonstrate that low-salinity waterflooding significantly improves microscopic sweep efficiency by enhancing the stability and rigidity of the oil-water interface. This enhancement is achieved through ion-regulated modifications of the interfacial film, particularly through the formation of hydration-bridged structures. Surface pressure-area isotherms, interfacial dilational rheology, and Zeta potential measurements show that the interfacial properties are highly dependent on the type and concentration of cations. Specifically, Mg^{2+} produces the most significant effects, leading to the highest collapse pressure ($53.7 \text{ mN}\cdot\text{m}^{-1}$), elastic modulus ($19.71 \text{ mN}\cdot\text{m}^{-1}$), and a significantly reduced Zeta potential (-13.77 mV), indicating a more stable and rigid interfacial film. These effects are attributed to the stronger interactions between Mg^{2+} and the carboxyl groups of stearic acid, which promote tighter molecular packing and interfacial elasticity. Furthermore, the increased interfacial elasticity observed at deformation frequencies between 0.025 and 0.1 Hz supports the formation of a viscoelastic nanomembrane that resists localized deformation under flow. This enhanced interfacial structure helps suppress viscous fingering, stabilize the displacement front, and improve displacement efficiency. As a result, low-salinity waterflooding, particularly with optimized cation concentrations, significantly enhances oil recovery by improving microscopic sweep efficiency in heterogeneous reservoirs. The study provides valuable insights into the mechanisms behind low-salinity waterflooding and highlights the critical role of ionic regulation in optimizing oil recovery processes.

Keywords: Surface pressure; Interfacial dilational rheology; Stability; Zeta potential; EOR

NONMENCLATURE

Abbreviations

LSWF Low-Salinity Waterflooding

LSW	Low-Salinity Water
IFT	Interfacial Tension
SA	Stearic Acid
FW	Formation Water
EOR	Enhanced Oil Recovery
NMR	Nuclear Magnetic Resonance
π -A	Surface Pressure–Molecular Area Isotherm
TDS	Total Dissolved Solids
Symbols	
π	Surface pressure
A	Average molecular area
G' , G''	Storage (elastic) modulus, Loss (viscous) modulus
ζ	Zeta potential
ϕ	Porosity
S_{or}	Residual oil saturation
T_1 , T_2	NMR relaxation times

1. INTRODUCTION

Low-salinity waterflooding (LSWF) has emerged as a cost-effective and environmentally sustainable enhanced oil recovery (EOR) technology, widely applied in both onshore and offshore reservoirs[1, 2]. Unlike conventional waterflooding that typically relies on high-salinity seawater or formation brine, LSWF involves modifying the ionic composition and salinity of injected brines to improve interactions among oil, water, and reservoir rock[3, 4]. Since its first field applications, LSWF has been shown to improve oil displacement efficiency, reduce residual oil saturation, and enhance sweep coverage without the need for costly chemical additives[5, 6].

The traditional mechanisms proposed for the success of LSWF include wettability alteration, ion exchange, mineral dissolution, pH modification, and moderate

[#] This is a paper for the 17th International Conference on Applied Energy (ICAE2025), December 8-12, 2025, Bangkok, Thailand.

reductions in interfacial tension (IFT)[7, 8]. Lowering the ionic strength of injected water expands the electrical double layer at the rock surface, weakens cation bridges between oil polar components and mineral surfaces, and promotes desorption of acidic species such as carboxylic acids and asphaltene aggregates[9]. These desorbed surface-active molecules migrate to the oil–water interface, facilitating the formation of interfacial films and occasionally microemulsions that mobilize trapped oil[10]. In carbonate reservoirs, where the mineral surface charge is often positive at reservoir conditions, sulfate ions (SO_4^{2-}) have been shown to act as “potential determining ions,” enhancing competitive adsorption and further promoting wettability alteration toward more water-wet conditions[11, 12]. However, these classical chemical explanations alone are insufficient to fully describe the complex pore-scale flow phenomena observed during LSWF[13, 14]. Micromodel and coreflood experiments have consistently demonstrated that low-salinity brines not only mobilize previously trapped oil clusters but also stabilize the displacement front, suppressing viscous fingering and improving microscopic sweep efficiency[15-17]. This flow stabilization suggests that, beyond static wettability and equilibrium IFT effects, dynamic interfacial mechanical properties play a critical role in regulating the oil–water displacement process[18, 19].

Recent studies have highlighted the importance of interfacial viscoelasticity as a key rheological property governing LSWF performance[20-22]. Interfacial viscoelasticity reflects the ability of the oil–water interface to store and dissipate mechanical energy under dynamic deformation. An interface with higher viscoelasticity can resist compression and extension, maintaining its structural integrity under shear flow, which leads to a more uniform and piston-like displacement front[23-25]. Conversely, a weakly viscoelastic interface is prone to breakup, facilitating the formation of unstable fingers and bypassed oil zones. Importantly, inorganic cations present in the brine strongly influence interfacial viscoelasticity. Monovalent ions such as Na^+ mainly provide electrostatic screening, while divalent cations such as Ca^{2+} and Mg^{2+} can form ionic bridges with carboxyl and phenolic groups in crude oil polar components, thereby enhancing interfacial molecular packing and elasticity[17, 26, 27]. Nevertheless, the relationship between ionic strength and interfacial viscoelasticity is highly non-linear. While moderate concentrations of Ca^{2+} and Mg^{2+} increase the surface collapse pressure and elastic modulus of interfacial films, excessively high ionic strength may

over-compress the electrical double layer, reducing molecular mobility and making the interface brittle[28, 29]. Thus, an optimal ion composition is needed to balance enhanced rigidity with sufficient flexibility to resist dynamic deformation. Despite increasing evidence linking brine composition to interfacial rheology, the fundamental mechanisms by which specific cations regulate interfacial viscoelasticity and their impact on pore-scale sweep efficiency remain poorly understood[30, 31]. In addition to ionic effects, reservoir heterogeneity and crude oil composition exert a profound influence on the LSWF response, particularly in the Middle Eastern offshore carbonate reservoirs[24, 25, 32]. Such compositional variability significantly affects wettability, IFT, emulsion stability, and the formation of interfacial viscoelastic structures, leading to variable and sometimes contradictory LSWF performance across different reservoir regions[33, 34]. Specifically, polar components of crude oil, such as asphaltenes and resins, play a dominant role in determining wettability and interfacial film properties[35, 36]. Higher polar content increases interfacial adsorption, strengthens viscoelastic films, and may enhance displacement stability under suitable conditions[37, 38]. However, excessive interfacial rigidity caused by high polarity can hinder mobilization and reduce oil recovery if not balanced by favorable flow conditions[39]. This complex interplay highlights the importance of considering oil composition when designing low-salinity brine formulations for carbonate reservoirs[40, 41]. Moreover, injection dynamics such as flow rate introduce another layer of complexity in LSWF. At low flow rates, capillary forces dominate, and wettability alteration is the primary recovery mechanism. At higher flow rates, viscous forces become significant, deforming the oil–water interface and promoting droplet elongation or detachment[42, 43]. The capillary number thus governs the transition between capillary-controlled and viscous-controlled regimes. However, excessively high flow rates can induce viscous fingering, reduce sweep efficiency, and bypass significant portions of the reservoir[44, 45]. Although several macroscopic studies have linked injection rate to recovery, few have systematically investigated the coupled effects of shear forces, crude oil polarity, and ion-regulated interfacial viscoelasticity on pore-scale flow stability[46-48]. In summary, the dynamic behavior of the oil–water interface under realistic reservoir conditions involves a complex interplay of ionic effects, crude oil polarity, and injection dynamics. While wettability alteration remains a primary mechanism, it alone cannot explain the improved microscopic sweep

and stabilized displacement fronts observed in LSWF. A deeper understanding of how ion-specific interactions modulate interfacial viscoelasticity, and how this rheological regulation couples with oil composition and flow dynamics, is crucial for advancing LSWF design in carbonate reservoirs.

This study aims to bridge these knowledge gaps by integrating multiscale experiments and numerical simulations to elucidate the dynamic recovery mechanisms of LSWF in carbonate reservoirs. Langmuir monolayer experiments with stearic acid as a model polar compound quantify the effects of Na^+ , Ca^{2+} , and Mg^{2+} on surface pressure, viscoelastic moduli (G' , G''), and Zeta potential. Carbonate-analog micromodel flooding visualizes the suppression of viscous fingering under optimized brine compositions, while low-field NMR characterizes residual oil redistribution and pore-scale saturation changes under varying injection rates. By establishing a mechanistic link between ion-specific interfacial rheology, crude oil polarity, and injection dynamics, this work provides new insights for designing “smart water” formulations and injection strategies tailored to the complex geological and compositional heterogeneity of Middle Eastern offshore carbonate reservoirs.

2. MATERIALS AND METHODS

2.1 Materials

Stearic acid (SA) was selected as a model compound to simulate the interfacial behavior of weakly acidic polar components in crude oil, owing to its simple structure and carboxyl headgroup, which resemble those of asphaltenes and resins. SA, aviation kerosene, and electrolytes (NaCl , CaCl_2 , MgCl_2) were purchased from Aladdin Reagent Co. with purities exceeding 99% (AR grade). Table I presents the composition and salinity of the brine solutions used in this study. Formation water (FW) and low-salinity water (LSW) were prepared in the laboratory using pure salts and deionized water, respectively. The ionic composition of the formation water was based on the composition of Middle East offshore oilfields. To eliminate anion effects, only chloride salts were used, isolating the influence of anion type and concentration on interfacial behavior. All solutions were prepared using ultrapure water (conductivity $< 0.055 \mu\text{S}/\text{cm}$) from a Seralpur Pro 90 system. Electrolyte concentrations are detailed in Table1.

Table 1. Ionic composition of the subphase solution used in the experiment.

Salt	Salt concentration (mg/L)					
NaCl	2000	4000	6000	10000	60000	
MgCl ₂	250	500	1250	2500	10000	
CaCl ₂	291	582	1457	2914	10000	

Injection water	Salt concentration (mg/L)							
	Na ⁺	K ⁺	Ca ²⁺	Mg ²⁺	Cl ⁻	SO ₄ ²⁻	HCO ₃ ⁻	Total dissolved solids
Formation water (FW)	75009.6	1170.9	13626.8	1748	145134.9	1116.7	422.7	238460.5
Low-salinity water (LSW)	3160	0	250	250	1000	3160	0	7820

2.2 Low-field NMR measurements

Low-field nuclear magnetic resonance (NMR, MesoMR23-060H, Niumag) was employed to monitor fluid redistribution in carbonate rock plugs during sequential brine flooding. Cores were first fully saturated with oil under vacuum. They were then subjected to flooding with formation water (FW) followed by low-salinity brines with different cation compositions. After each flooding stage, NMR T_2 spectra were collected to quantify movable and residual oil. Additionally, 2D T_1 - T_2 maps were used to distinguish oil/brine distribution in macropores versus micropores, allowing direct assessment of microscopic sweep efficiency improvements. Based on the response of different hydrogen-bearing materials and in conjunction with the

results from Zhang et al.[49], He et al.[50], Ma et al.[51], Liu et al.[52], a discriminating plate (Fig. 1) was summarized to analyze the distribution of water and oil.

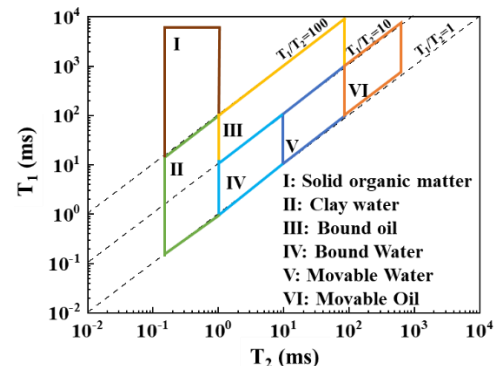


Fig. 1 Identification graph of hydrogen-bearing matter distribution in T_1 - T_2 spectra[50].

2.3 Microfluidic displacement visualization

To evaluate the effect of ion-regulated interfacial rheology on pore-scale flow stability, displacement visualization experiments were conducted using a fabricated micromodel (Fig. 2). Prior to each test, the micromodel was thoroughly cleaned with ethanol and deionized water, dried under vacuum, and rendered oil-wet by pre-flooding with SA-containing model oil at 0.1 mL/min for 12 h, followed by aging for 24 h at 60 °C. Subsequently, the micromodel was flooded with brine solutions containing Na^+ , Ca^{2+} , or Mg^{2+} at varying concentrations, with injection rates corresponding to capillary numbers between 10^{-6} and 10^{-3} . A high-resolution optical microscope equipped with a CCD camera recorded the evolution of the displacement front at 5 frames/s, and the acquired images were analyzed using ImageJ software to quantify residual oil saturation (S_{or}).

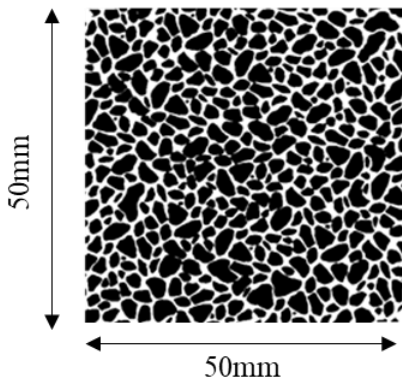


Fig. 2 The seepage model structure.

2.4 Langmuir monolayer experiments

Surface pressure-area (π - A) isotherms and interfacial dilatational rheology were measured using a KSV-NIMA Langmuir trough (PTFE material, Finland, Fig.3). The trough was cleaned with ethanol, chloroform, and ultrapure water before use. Experiments began after surface pressure stabilized (fluctuations $< 0.5 \text{ mN}\cdot\text{m}^{-1}$). A stock solution was prepared by dissolving 3 g of SA in 20 mL of chloroform (CHCl_3). A 20 μL aliquot was spread onto the salt solution subphase (liquid height 2-3 mm above barriers). After chloroform evaporation, the monolayer was compressed at 10 mm/min to obtain π - A isotherms (Fig. 4)[53, 54]. Oscillatory compression at 0.005, 0.025, and 0.1 Hz was applied to assess

dilatational rheology. The experimental temperature was maintained at $(23 \pm 1) \text{ }^\circ\text{C}$.

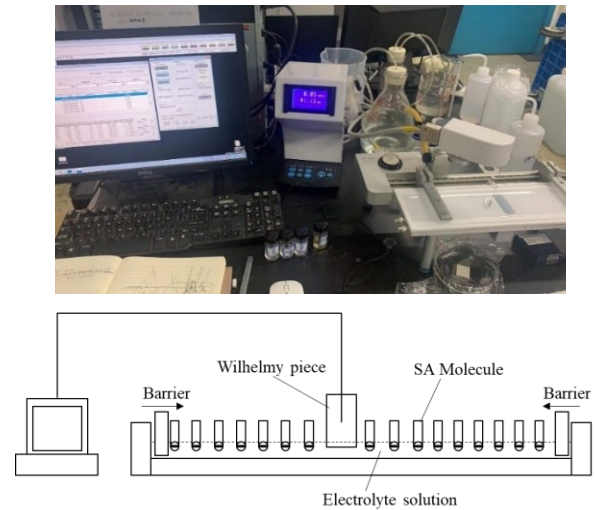


Fig. 3 Langmuir trough set-up (KSV-NIMA, Finland), and the schematic diagram of the surface film pressure experiment at the oil-water interface

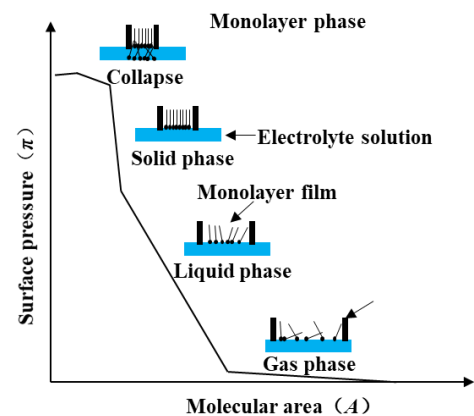


Fig. 4 Typical surface pressure(π)-molecular area(A) curve.

2.5 Zeta potential measurements

Zeta potential measurements were performed using a Zetasizer Nano ZS (laser Doppler microelectrophoresis). The model oil was prepared by dissolving 0.5 g of SA in 100 mL of aviation kerosene at 60 °C. Then, 1 mL of model oil was mixed with 50 mL of salt solutions containing 0.5 mol of SA. After stirring (1200 rpm, 2 h), ultrasonication (2 h), and settling (1 h), emulsions were analyzed. Each sample was tested 6 times, averaging five cycles, to determine the Zeta potential.

3. RESULTS AND DISCUSSION

3.1 NMR spectra characteristics

Fig. 5 shows the changes in the T_1 - T_2 2D NMR spectra of the core during the low-salinity waterflooding experiment, covering four main stages: water saturation, oil saturation, formation water flooding, and low-salinity water flooding. In the water-saturated stage (Fig. 5a), the NMR signal is primarily distributed in the IV and V regions, indicating that the core mainly contains movable water and adsorbed water [50]. With the injection of oil, in the oil-saturated stage (Fig. 5b), the NMR signal is mainly concentrated in the VI region, reflecting changes in the oil distribution. The crude oil, due to its stronger polarity, may adsorb onto the core surface, causing some organic solids to enter the core pores, which increases the signal intensity in the I region. In the formation water flooding stage (Fig. 5c), formation water displaces the movable oil in the large pores, and the NMR signal decreases in the VI region, shifting to the IV and V regions. This indicates that formation water effectively replaced the oil phase, leaving behind a small amount of solid organic matter and immobile residual oil.

Compared to low-polarity crude oil, high-polarity crude oil, due to its stronger hydrophilicity, is more easily adsorbed onto the core surface, resulting in some oil molecules being difficult to displace. In the low-salinity water flooding stage (Fig. 5d), low-salinity water further displaces the residual oil in both large and small pores. The NMR signal weakens in the VI region, while the signal in the IV and V regions significantly increases, indicating that low-salinity water not only successfully replaced the residual oil in the large pores but also penetrated into the small pores, replacing the oil phase there. This process demonstrates that low-salinity water significantly improves the oil-water distribution and enhances oil displacement efficiency, especially in the small pores[55]. Low-salinity waterflooding shows a significant advantage in the recovery of crude oil. Low-salinity water improves oil recovery by altering wettability, reducing interfacial tension, and promoting oil-water phase exchange, thus optimizing the displacement process.

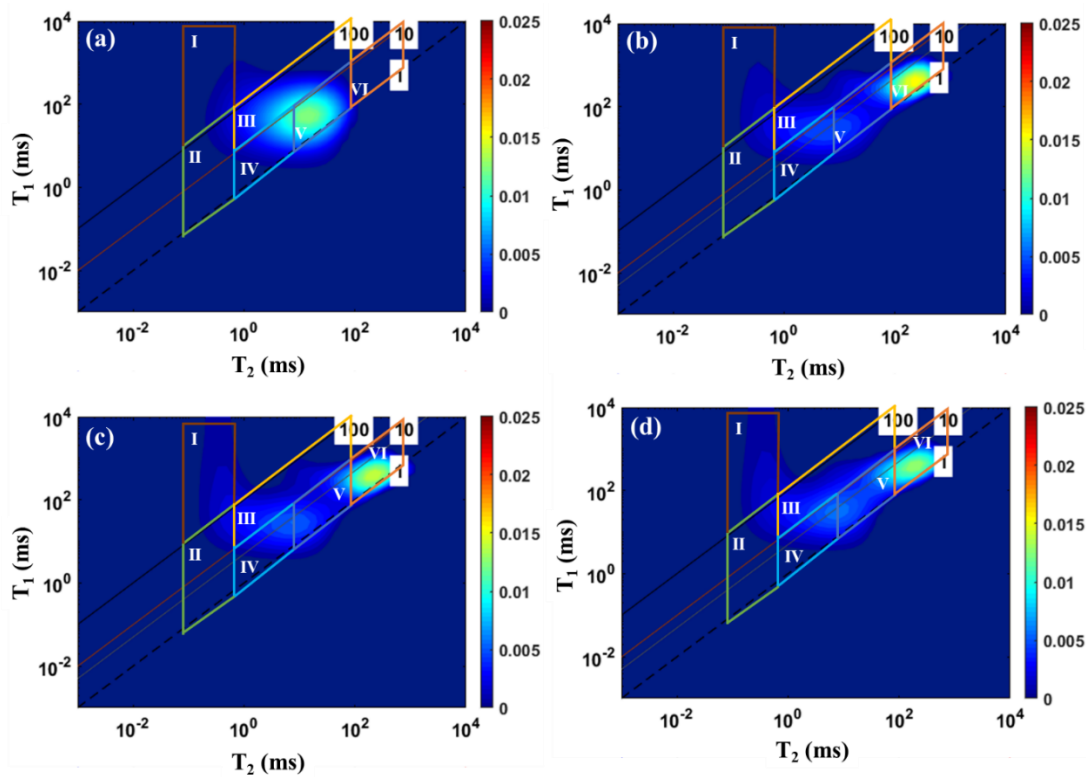


Fig. 5 2D T_1 - T_2 spectra after normalization at different experimental stages, with experimental results for crude oil with high polar content on the left. (a) Water saturated sample; (b) Oil saturated sample (in the presence of immobile water); (c) Formation water flooded sample; (d) Low-salinity water flooded sample[50].

3.2 Oil-water distribution characteristics

Fig. 6 shows the changes in oil-water distribution of the high-polarity crude oil model during formation water flooding (FW) and low-salinity water flooding (LSW). Figs.

6a and 6b indicate that during formation water flooding, due to the wettability of crude oil with the rock surface and the inherent heterogeneity of the rock pores, fingering occurs. Water preferentially invades larger pores and throats, forming main flow channels (I), which

leads to the accumulation of a large amount of residual oil. The residual oil is adsorbed on the oil film layer on the pore surface (blue arrow in Fig. 6b), with the oil recovery rate at this point being 25.24%. As shown in Figs. 6c and 6d, after the injection of low-salinity water, water further penetrates small pores along high-permeability pathways and displaces the oil film. The oil film on the pore surface is dissolved and thinned by the water flow, and the remaining oil is displaced (red arrow in Fig. 6d). Water drives the oil film along the pore

surface (blue arrow), resulting in an increased recovery rate of approximately 49.73%. Low-salinity water significantly improves the oil-water distribution, particularly enhancing oil-water exchange in small pores. The advantage of low-salinity water is not only reflected in changes in permeability and wettability but also in the dissolved ions (such as Na^+ , Ca^{2+} , Mg^{2+}) in the water. These ions may regulate the mechanical properties of the oil-water interface, further improving oil displacement efficiency [50].

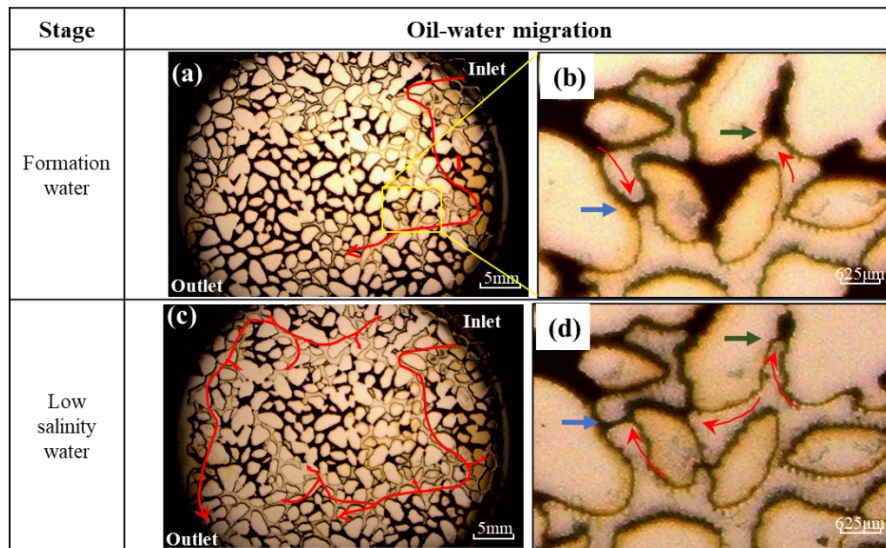


Fig. 6 Oil-water migration of crude oil model at different flooding stages[50].

3.3 Surface Pressure-Average Molecular Area Characteristics of Stearic Acid Monolayers

The surface pressure-average molecular area (π -A) characteristics of stearic acid (SA) monolayers were investigated in NaCl , CaCl_2 , and MgCl_2 solutions at varying concentrations. As shown in Fig. 7, the collapse pressure displayed a non-monotonic trend: increasing to a peak at intermediate concentrations and then declining with further ion addition. This behavior suggests an optimal ion concentration range for film stability, consistent with the Schulze-Hardy rule[56]. At low concentrations, cations compress the electrical double layer(Gouy-Chapman theory[57]), enhancing SA molecular cohesion. For NaCl , the highest collapse pressure appears at 2000 mg/L[58, 59], after which excessive Na^+ causes double-layer overcompression and Zeta potential rebound, weakening film stability.

In contrast, divalent cations Ca^{2+} and Mg^{2+} interact more strongly with $-\text{COOH}$ groups, enhancing structural stability. Ca^{2+} forms inner-sphere complexes and Ca^{2+} -SA- Ca^{2+} bridges[60], but at 10000 mg/L, excessive Ca^{2+} induces dense, brittle films with reduced flexibility. Mg^{2+} ,

with higher hydration energy and a smaller hydrated radius[61, 62], forms hydration-mediated bridges that preserve solid-liquid coexistence even at higher concentrations. Mg^{2+} achieves the highest collapse pressure ($53.7 \text{ mN}\cdot\text{m}^{-1}$), indicating a robust yet elastic interfacial network. Structural reorganization during compression highlights ion-specific effects. In ultrapure water, SA monolayers exhibit typical gas-liquid-solid transitions. High Ca^{2+} concentrations disrupt this, causing premature solidification, whereas Mg^{2+} preserves molecular mobility and enhances elasticity.

Low-salinity water can alter the strength of the oil-water interface by adjusting the ionic composition, thereby regulating the microscopic sweep efficiency. Moderate salt concentrations optimize double-layer compression, while excessive ions destabilize films. Mg^{2+} 's superior bridging supports stable nanofilm formation. Enhanced interfacial rigidity under optimal conditions suppresses capillary fingering and promotes piston-like front advancement, improving microscopic sweep efficiency in heterogeneous reservoirs. These insights are also consistent with classical Langmuir-Blodgett monolayer theory, which emphasizes the

relationship between molecular packing, surface pressure, and film collapse behavior[63, 64]. Moreover, the evolution of collapse pressure under different ionic conditions provides critical guidance for oil displacement processes during low salinity waterflooding. A higher collapse pressure indicates a more robust interfacial film capable of resisting flow-induced deformation. This

enhanced interfacial strength suppresses capillary fingering, stabilizes the displacement front, and promotes piston-like oil displacement. Thus, optimizing ionic regulation of interfacial mechanics directly contributes to improving microscopic sweep efficiency and enhancing the effectiveness of low salinity waterflooding operations.

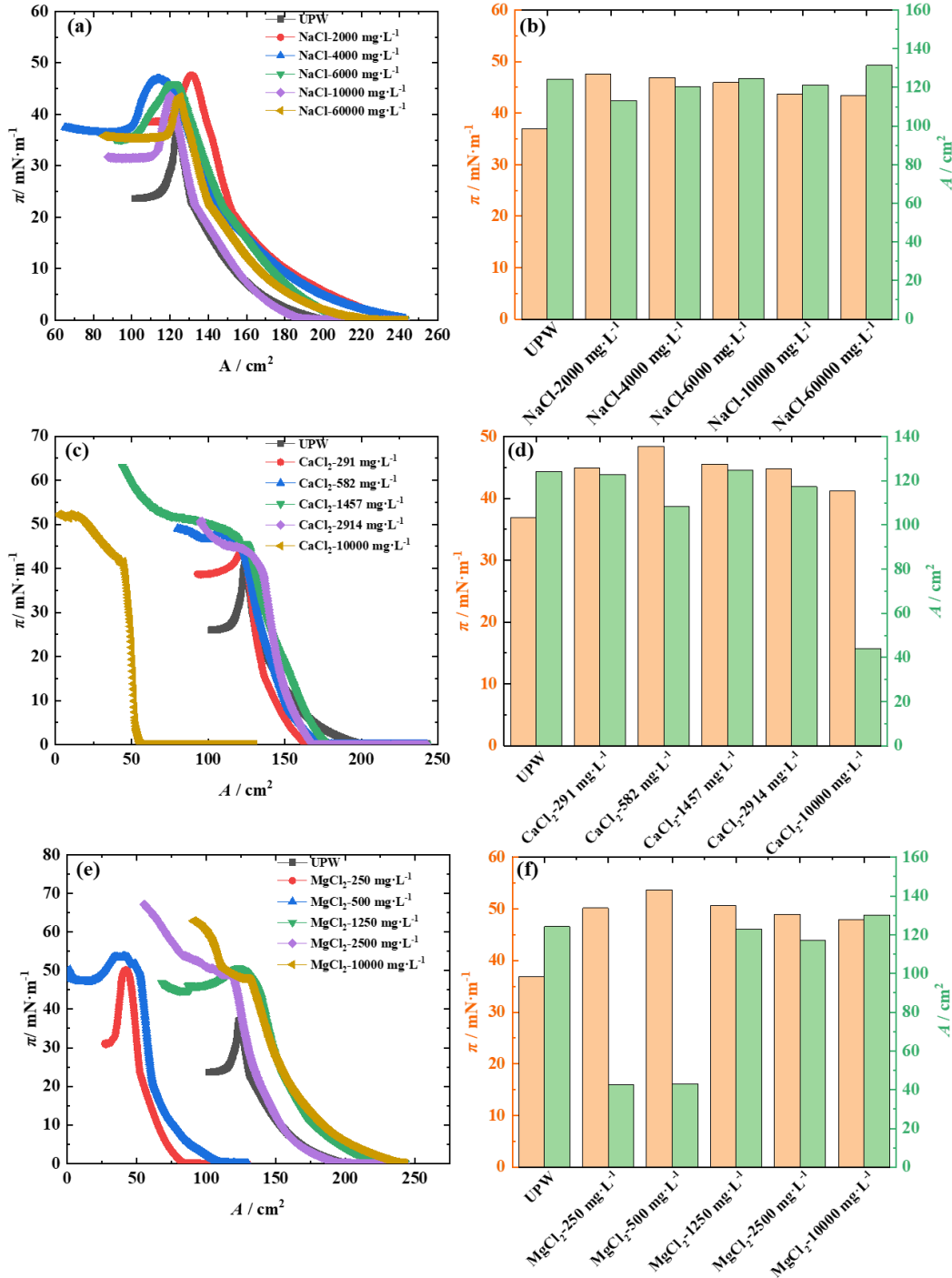


Fig. 7 π - A isotherm curves, collapse pressure, and corresponding molecular area of stearic acid on different electrolyte solutions, (a, b) NaCl solution; (c, d) CaCl_2 solution; (e, f) MgCl_2 solution.

3.4 Viscoelastic Behavior of Stearic Acid Monolayers

The viscoelastic behavior of stearic acid monolayers under varying cation concentrations (Na^+ , Ca^{2+} , Mg^{2+}) is shown in Fig. 8. For all ions, both the elastic and viscous moduli initially increase with concentration, reaching a maximum before declining at higher concentrations, consistent with ion-specific modulation of interfacial

properties[56]. Na^+ ions, due to their monovalent nature, weakly interact with the carboxyl headgroups of SA, resulting in slight improvements in modulus at low concentrations but moderate declines thereafter, reflecting limited impact on film structure.

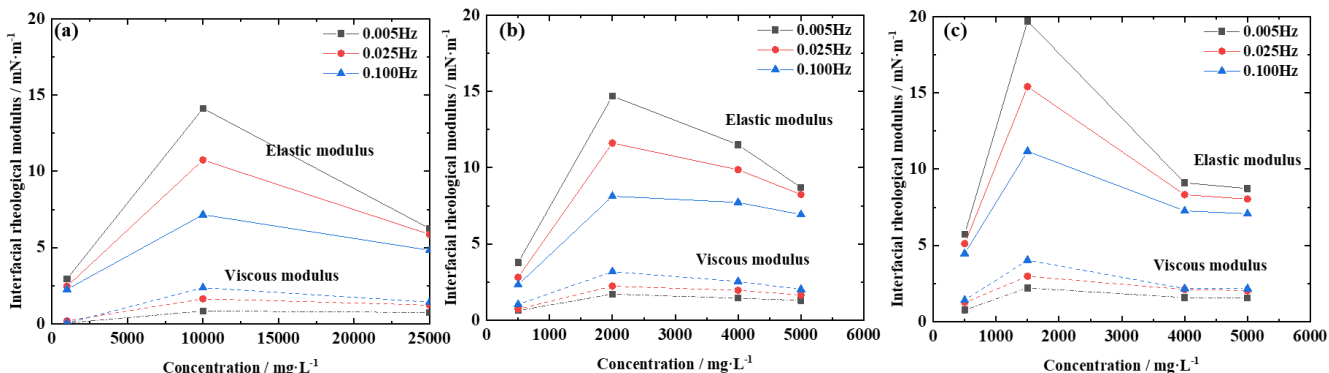


Fig. 8 Elastic modulus and viscous modulus of stearic acid on different electrolyte solutions, (a) NaCl solution; (b) CaCl₂ solution; (c) MgCl₂ solution.

In contrast, divalent Ca^{2+} and Mg^{2+} significantly enhance the elastic and viscous moduli at low to moderate concentrations. Mg^{2+} shows a superior effect even at lower concentrations, attributed to its higher hydration energy and smaller hydrated radius, which facilitate stronger hydration-mediated bridging between carboxylic groups[61]. This bridging not only enhances molecular packing but also preserves partial flexibility, allowing the film to store more deformation energy. At higher concentrations, overcompensation and excessive ion adsorption reduce surface charge repulsion and disrupt the interfacial structure, leading to sharp modulus declines. This effect is more pronounced for Mg^{2+} , while Ca^{2+} induces a more gradual destabilization due to its larger hydration radius. Across all frequencies tested (0.025-0.1 Hz), the elastic modulus (G') consistently exceeds the viscous modulus (G''), indicating that the films maintain a high-resistance, elasticity-dominated character. The strongest elastic response is observed at 0.05 Hz, suggesting that at lower deformation rates, the films better resist structural disruption.

Similarly, low-salinity water can modify the viscoelasticity of the oil–water interface through ionic composition adjustment, thus regulating the microscopic sweep efficiency. Enhanced interfacial elasticity, particularly under Mg^{2+} regulation at moderate concentrations (1500-2000 mg/L), suppresses viscous fingering, stabilizes the displacement front, and improves microscopic sweep efficiency[63, 64]. In contrast, excessive cation concentrations lead to film

collapse, highlighting the need for ion adjustment. The results demonstrate that modulating interfacial viscoelasticity through specific ionic composition can regulate the mobility ratio and optimize displacement uniformity in heterogeneous porous media.

3.5 Zeta Potential Analysis and Membrane Stability

As shown in Fig. 9, the Zeta potential analysis in NaCl, CaCl₂, and MgCl₂ solutions reveals how different cations influence interfacial charge neutralization and membrane stability. In NaCl solutions, the Zeta potential decreases as Na^+ concentration rises, suggesting effective neutralization of the crude oil surface charge. However, at concentrations above 14610 mg/L, the neutralization effect saturates, and the Zeta potential slightly increases, indicating a weakened charge neutralization. In contrast, Ca^{2+} and Mg^{2+} , as divalent cations, exhibit stronger charge neutralization, reducing electrostatic repulsion more effectively. In CaCl₂ and MgCl₂ solutions, the Zeta potential increases significantly with concentration, showing stronger interactions with the crude oil surface due to their higher charge density and smaller ionic radii. This results in enhanced membrane stability, as these cations form stronger coordination bonds with stearic acid molecules, increasing membrane strength and compactness. At moderate concentrations, the coordination effects of Ca^{2+} and Mg^{2+} notably improve membrane structural integrity, reducing repulsion and enhancing film stability. The stronger charge neutralization and structural

enhancement at these concentrations lead to greater membrane resistance and strength.

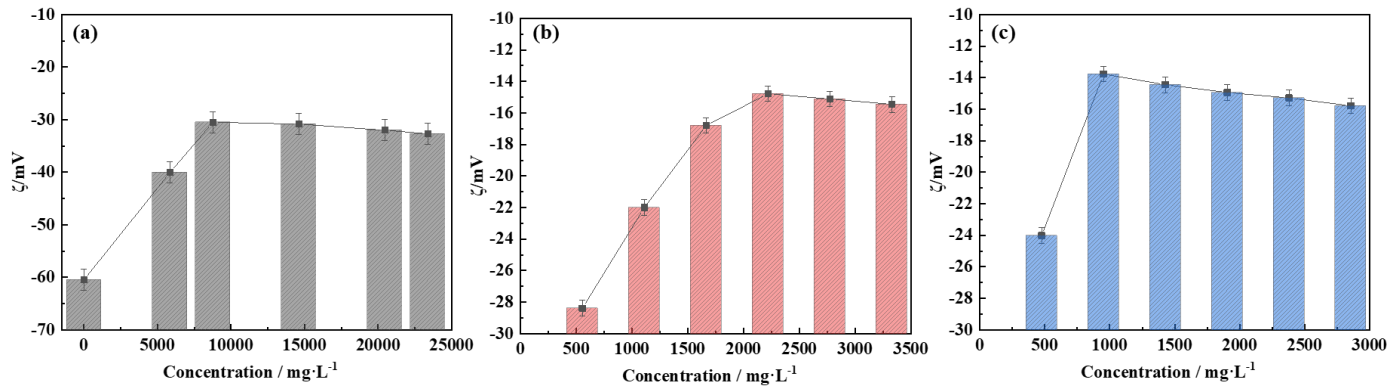


Fig. 9 Zeta potential of oil-water systems in electrolyte solutions of different concentrations, (a) NaCl solution; (b) CaCl₂ solution; (c) MgCl₂ solution.

These interfacial charge dynamics are particularly important in the context of low salinity waterflooding, where the regulation of Zeta potential directly affects the formation and stability of viscoelastic interfacial films. When the interface is more fully neutralized by a moderate concentration of divalent cations, electrostatic repulsion between interfacial molecules is reduced. This reduction promotes closer molecular packing and enhances intermolecular cohesion, thereby improving the structural integrity of the interfacial film. This compact interface can better withstand shear deformation and maintain continuity under flow, which is critical for controlling the displacement front within porous media. From a reservoir engineering perspective, such charge-regulated stabilization suppresses localized interfacial disruption and minimizes flow channeling through high-permeability zones.

3.6 The Effect of Ion Regulation on the Microscopic Sweep Efficiency of Low-Salinity Water Flooding

The experimental results highlight the significant role of electrolyte type and concentration in regulating the rheology and stability of stearic acid films. This study introduces an alternative mechanism: the in-situ formation of surfactant-like structures at the oil-water interface via cation coordination. These nanostructures create a viscoelastic barrier, promoting piston-like displacement, a mechanism distinct from traditional capillary-driven oil recovery[35, 65]. While conventional models attribute improved oil recovery solely to interfacial tension reduction and wettability alteration[66], the interfacial rheology data in this study indicate that increased interfacial rigidity suppresses

viscous fingering, thereby controlling displacement efficiency[67]. This behavior is analogous to the viscoelastic mechanism observed in polymer flooding[68], and the piston-like displacement mechanism is illustrated in Fig. 10. The divalent cations (Ca²⁺, Mg²⁺) outperform Na⁺ in enhancing interfacial film rigidity due to their higher charge density and hydration properties. At low concentrations, Ca²⁺ and Mg²⁺ effectively neutralize the Zeta potential of stearic acid carboxyl (-COOH) groups by forming stable coordination bonds, consistent with previous findings[69, 70]. However, excessively high cation concentrations, particularly those of divalent cations, can result in charge overcompensation, which disrupts the integrity of interfacial nanostructures. Specifically, Mg²⁺, due to its larger hydration radius[71], is more effective in bridging adjacent stearic acid molecules at moderate concentrations, significantly increasing the elastic modulus of the interface[72]. This explains the observed stability ranking: Mg²⁺ > Ca²⁺ > Na⁺. When injection water containing divalent cations (Ca²⁺, Mg²⁺) interacts with crude oil polar components, the resulting nanoaggregates form a continuous viscoelastic film at the oil-water interface. This nanofilm uniformly transmits pressure and resists localized deformation during displacement. As shown in Fig. 10b, in capillary models, conventional waterflooding results in interfacial instability, forming multi-branched fingering channels (Fig.10a, red arrows), whereas in this system, the viscoelastic interface facilitates a more uniform and frontally stable displacement (Fig. 10b, red arrows), thereby reducing residual oil saturation.

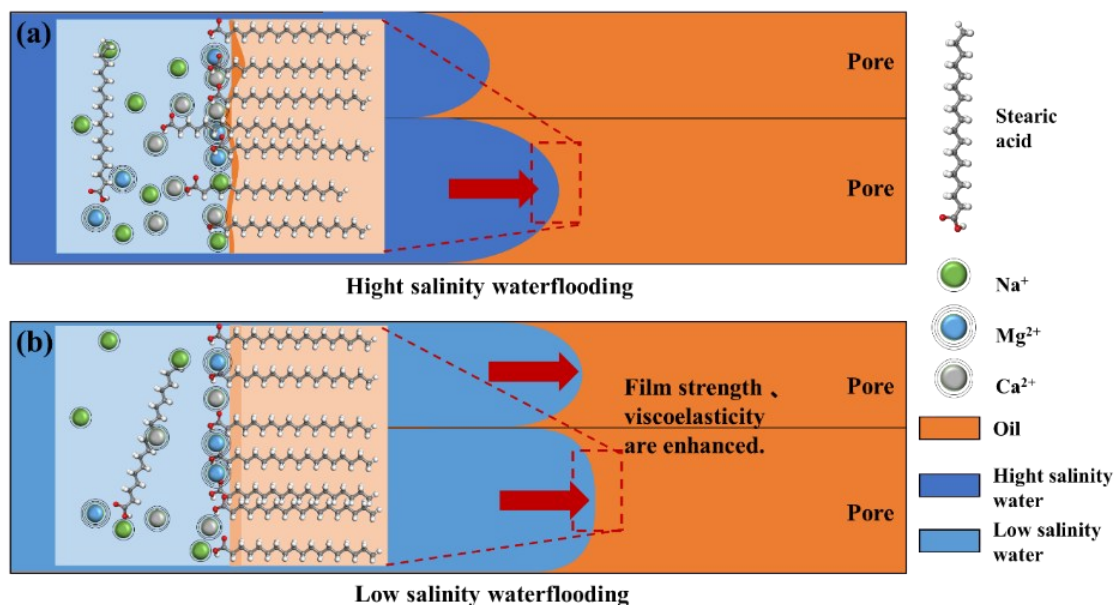


Fig. 10 Mechanism of oil recovery efficiency enhancement by interfacial strength and viscoelasticity changes in low salinity waterflooding.

This self-assembled ion nanostructure mechanism eliminates the need for additional chemical additives. Field applications should optimize cation composition rather than solely reducing salinity. For calcium-rich reservoirs (e.g., North Sea chalk formations[73, 74]), Mg^{2+} injection can synergize with formation divalent cations to enhance interfacial film strength. Conversely, in sodium-dominated reservoirs, careful Mg^{2+} , Ca^{2+} dosing is required to enhance oil-water interfacial strength while preventing clay swelling.

The experimental findings demonstrate that different cations regulate the structure of the interfacial film through a combination of electrostatic screening, double-layer compression, and molecular coordination. Among these, divalent cations such as Mg^{2+} exhibit the most pronounced effects, especially at moderate concentrations, where they achieve optimal interfacial stability and enhanced elastic modulus. This indicates that their influence is not limited to simple charge neutralization at the molecular scale but also involves specific interactions between hydrated cation structures and polar functional groups. The resulting evolution of the interfacial microstructure contributes to the suppression of viscous fingering and promotes the stability of the displacement front during fluid flow. These effects collectively enhance microscopic sweep efficiency and provide a solid physicochemical basis for improving the performance of low-salinity waterflooding.

4. CONCLUSION

This study investigates the effect of low-salinity waterflooding on enhanced oil recovery, focusing on the role of different cations (such as Ca^{2+} , Mg^{2+} , and Na^{+}) on the interfacial structure and viscoelastic properties of the oil monolayers under low-salinity waterflooding conditions, with a focus on how cation-induced modifications of interfacial film behavior influence microscopic sweep efficiency. This study provides practical insights for enhancing oil recovery in heterogeneous reservoirs and suggests that cation composition optimization is key for improving the effectiveness of low-salinity waterflooding. The main conclusions are as follows:

1. The NMR spectra analysis shows that low-salinity water significantly improves the oil-water distribution in the core, especially in small pores. The displacement efficiency is notably higher compared to formation water flooding.

2. During low-salinity waterflooding, water effectively penetrates small pores and displaces the oil film, resulting in an increased oil recovery rate (49.73%) compared to formation water flooding (25.24%).

3. Low-salinity water enhances the stability and strength of the oil-water interfacial film by adjusting the electrolyte composition, with divalent cations (Ca^{2+} and Mg^{2+}) playing a significant role in improving film stability.

4. The viscoelastic behavior of the oil-water interface changes during low-salinity waterflooding, suppressing viscous fingering and promoting uniform front

movement, which improves microscopic sweep efficiency.

5. By optimizing the cation concentrations, particularly Mg^{2+} and Ca^{2+} , the interfacial strength is enhanced, leading to improved oil recovery without the need for additional chemical additives.

ACKNOWLEDGEMENT

Supported by the National Natural Science Foundation of China (Grant No.52274048); the National Major Science and Technology Projects of China (No. 2017ZX05032004-002); the Major Science and Technology Projects of PetroChina (No. 2020D-5007-0203) and the Shaanxi Province Technology Innovation Guidance Special Plan Project (No. 2023-YD-CGZH-02).

REFERENCE

[1] Almeida da Costa A, Trivedi J, Soares J, et al. An experimental evaluation of low salinity water mechanisms in a typical Brazilian sandstone and light crude oil with low acid/basic number. *Fuel* 2020;273. <https://doi.org/10.1016/j.fuel.2020.117694>

[2] Derkani M, Fletcher A, Abdallah W, et al. Low Salinity Waterflooding in Carbonate Reservoirs: Review of Interfacial Mechanisms. *Colloids and Interfaces* 2018;2(2). <https://doi.org/10.3390/colloids2020020>

[3] Hossain MM, Imura KI. Interactions of L-arginine with Langmuir monolayers of common phospholipids at the air-water interface. *Chem Phys Lipids* 2021;235:105054. <https://doi.org/10.1016/j.chemphyslip.2021.105054>

[4] Bielejewska N, Hertmanowski R. Surface characterization of nanocomposite Langmuir films based on liquid crystals and cellulose nanocrystals. *Journal of Molecular Liquids* 2021;323. <https://doi.org/10.1016/j.molliq.2020.115065>

[5] Feng H, Kang W, Wu H, et al. Study on the relationship between emulsion stability and droplet dynamics of a spontaneous emulsion for chemical enhanced oil recovery. *Journal of Dispersion Science and Technology* 2017;39(8):1214-22. <https://doi.org/10.1080/01932691.2017.1391699>

[6] Emami H, Ayatizadeh Tanha A, Khaksar Manshad A, et al. Experimental Investigation of Foam Flooding Using Anionic and Nonionic Surfactants: A Screening Scenario to Assess the Effects of Salinity and pH on Foam Stability and Foam Height. *ACS Omega* 2022;7(17):14832-47. <https://doi.org/10.1021/acsomega.2c00314>

[7] Derikvand Z, Rezaei A, Parsaei R, et al. A mechanistic experimental study on the combined effect

of Mg^{2+} , Ca^{2+} , and SO_4^{2-} ions and a cationic surfactant in improving the surface properties of oil/water/rock system. *Colloids and Surfaces A: Physicochemical and Engineering Aspects* 2020;587. <https://doi.org/10.1016/j.colsurfa.2019.124327>

[8] Siadatifar SE, Fatemi M, Masihi M. Pore scale visualization of fluid-fluid and rock-fluid interactions during low-salinity waterflooding in carbonate and sandstone representing micromodels. *Journal of Petroleum Science and Engineering* 2021;198:108156. <https://doi.org/https://doi.org/10.1016/j.petrol.2020.108156>

[9] Tetteh JT, Barati R. Crude-Oil/Brine Interaction as a Recovery Mechanism for Low-Salinity Waterflooding of Carbonate Reservoirs. *SPE Reservoir Evaluation & Engineering* 2018;22(03):877-96. <https://doi.org/10.2118/194006-PA> %J *SPE Reservoir Evaluation & Engineering*

[10] Khajepour H, Akhlaghi Amiri HA, Ayatollahi S. Ion types effect on oil sweep efficiency during engineered waterflooding; an experimental micro-scale study. *Geoenergy Science and Engineering* 2024;241. <https://doi.org/10.1016/j.geoen.2024.213175>

[11] Chen B, Zhao L, Zhang N, et al. Mechanism analysis of injection technique of water composition modification for enhanced oil recovery. *Energy Sources, Part A: Recovery, Utilization, and Environmental Effects* 2024;46(1):6415-27. <https://doi.org/10.1080/15567036.2024.2347423>

[12] Mehraban MF, Farzaneh SA, Sohrabi M. Debunking the impact of salinity on crude oil/water interfacial tension. *Energy & Fuels* 2021;35(5):3766-79.

[13] Sun J, Xiu Z, Li L, et al. Application status and prospect of ionic liquids in oilfield chemistry. *Petroleum* 2024;10(1):11-8. <https://doi.org/10.1016/j.petlm.2023.08.001>

[14] Sun C, Liu M, Xu S, et al. Ion-induced oil–water wettability alteration of rock surfaces. Part I: Polar interactions between oil and solid. *Chemical Engineering Science* 2021;232. <https://doi.org/10.1016/j.ces.2020.116366>

[15] Zhu S, Tang K, Liu M, et al. Ion-induced oil–water wettability alteration of rock surfaces. Part III: Ion-bridging interactions between oil and solid. *Chemical Engineering Science* 2022;252. <https://doi.org/10.1016/j.ces.2021.117275>

[16] Belhaj AF, Singh N, Sarma HK. Understanding the Interactions at Rock-Water and Oil-Water Interfaces during Controlled-Salinity Water Flooding. *Offshore Technology Conference Asia*. Day 4 Fri, March 25, 2022. 2022.

- [17] Chai R, Liu Y, He Y, et al. Effects and Mechanisms of Acidic Crude Oil–Aqueous Solution Interaction in Low-Salinity Waterflooding. *Energy & Fuels* 2021;35(12):9860-72. <https://doi.org/10.1021/acs.energyfuels.1c00654>
- [18] Zhang X, Zhang T, Ge J, et al. The CO₂-in-water foam stabilized with the mixture of CO₂-soluble surfactant and nonionic surfactant. *Journal of Petroleum Science and Engineering* 2021;198. <https://doi.org/10.1016/j.petrol.2020.108117>
- [19] Li S, Li S, Wen N, et al. Highly effective removal of lead and cadmium ions from wastewater by bifunctional magnetic mesoporous silica. *Separation and Purification Technology* 2021;265:118341. <https://doi.org/10.1016/j.seppur.2021.118341>
- [20] Honarvar B, Rahimi A, Safari M, et al. Favorable attributes of low salinity water aided alkaline on crude oil-brine-carbonate rock system. *Colloids and Surfaces A: Physicochemical and Engineering Aspects* 2020;585:124144. <https://doi.org/10.1016/j.colsurfa.2019.124144>
- [21] Gonzales RR, Abdel-Wahab A, Adham S, et al. Salinity gradient energy generation by pressure retarded osmosis: A review. *Desalination* 2021;500:114841. <https://doi.org/10.1016/j.desal.2020.114841>
- [22] Kim J, Hong S. Pilot study of emerging low-energy seawater reverse osmosis desalination technologies for high-salinity, high-temperature, and high-turbidity seawater. *Desalination* 2023;565:116871. <https://doi.org/10.1016/j.desal.2023.116871>
- [23] Jawed AS, Nassar L, Hegab HM, et al. Recent developments in solar-powered membrane distillation for sustainable desalination. *Heliyon* 2024;10(11):e31656. <https://doi.org/10.1016/j.heliyon.2024.e31656>
- [24] Chen M, Cheng L, Lu T. Pore structure characterization and its impact on waterflooding development in Khasib reservoir in Ahdeb Oilfield, Iraq. *Lithologic Reservoirs* 2020;32(3):133-43.
- [25] Wang Q, Wen T, Li H, et al. Influence of heterogeneity on fluid property variations in carbonate reservoirs with multistage hydrocarbon accumulation: A case study of the Khasib formation, Cretaceous, AB oilfield, southern Iraq. *Open Geosciences* 2022;14(1):663-74. <https://doi.org/10.1515/geo-2022-0363>
- [26] Montazeri M, Fazelabdolabadi B, Shahrabadi A, et al. An experimental investigation of smart-water wettability alteration in carbonate rocks – oil recovery and temperature effects. *Energy Sources, Part A: Recovery, Utilization, and Environmental Effects* 2020;46(1):7798-810. <https://doi.org/10.1080/15567036.2020.1759735>
- [27] Liteanu E, Spiers CJ, de Bresser JHP. The influence of water and supercritical CO₂ on the failure behavior of chalk. *Tectonophysics* 2013;599:157-69. <https://doi.org/10.1016/j.tecto.2013.04.013>
- [28] Choi B-Y, Shinn Y-J, Park Y-C, et al. Simulation of CO₂ injection in a small-scale pilot site in the Pohang Basin, Korea: Effect of dissolution rate of chlorite on mineral trapping. *International Journal of Greenhouse Gas Control* 2017;59:1-12. <https://doi.org/10.1016/j.ijggc.2017.02.001>
- [29] Abdi A, Awarke M, Malayeri MR, et al. Interfacial tension of smart water and various crude oils. *Fuel* 2024;356:129563. <https://doi.org/10.1016/j.fuel.2023.129563>
- [30] Wei B, Lu L, Li Q, et al. Mechanistic Study of Oil/Brine/Solid Interfacial Behaviors during Low-Salinity Waterflooding Using Visual and Quantitative Methods. *Energy & Fuels* 2017;31(6):6615-24. <https://doi.org/10.1021/acs.energyfuels.7b00825>
- [31] Lashkarbolooki M, Ayatollahi S, Riazi M. The Impacts of Aqueous Ions on Interfacial Tension and Wettability of an Asphaltenic–Acidic Crude Oil Reservoir during Smart Water Injection. *Journal of Chemical & Engineering Data* 2014;59(11):3624-34. <https://doi.org/10.1021/je500730e>
- [32] Al-Ameri TK, Al-Temimi AK, Zumberge J. Assessments of oil characterization, source affinities, and hydrocarbon dynamic of East Baghdad oil fields, Central Iraq. *Marine and Petroleum Geology* 2016;77:353-75. <https://doi.org/10.1016/j.marpetgeo.2016.03.009>
- [33] Song C, Yoo H, Lee J. Effects of nano-smart water on enhanced oil recovery in carbonate reservoirs: Interfacial tension reduction and wettability alteration. *Colloids and Surfaces A: Physicochemical and Engineering Aspects* 2024;696:134362. <https://doi.org/10.1016/j.colsurfa.2024.134362>
- [34] Kar T, Cho H, Firoozabadi A. Assessment of low salinity waterflooding in carbonate cores: Interfacial viscoelasticity and tuning process efficiency by use of non-ionic surfactant. *J Colloid Interface Sci* 2022;607(Pt 1):125-33. <https://doi.org/10.1016/j.jcis.2021.08.028>
- [35] Mahmoudvand M, Javadi A, Pourafshary P, et al. Effects of cation salinity on the dynamic interfacial tension and viscoelasticity of a water-oil system. *Journal of Petroleum Science and Engineering* 2021;206:108970. <https://doi.org/10.1016/j.petrol.2021.108970>
- [36] Lv J, Xue K, Zhang Z, et al. Pore-scale investigation of hydrate morphology evolution and seepage characteristics in hydrate bearing microfluidic

- chip. *Journal of Natural Gas Science and Engineering* 2021;88:103881.
<https://doi.org/10.1016/j.jngse.2021.103881>
- [37] Rahimi A, Honarvar B, Safari M. The role of salinity and aging time on carbonate reservoir in low salinity seawater and smart seawater flooding. *Journal of Petroleum Science and Engineering* 2020;187:106739.
<https://doi.org/10.1016/j.petrol.2019.106739>
- [38] Yan L, Aslannejad H, Hassanizadeh SM, et al. Impact of water salinity differential on a crude oil droplet constrained in a capillary: Pore-scale mechanisms. *Fuel* 2020;274:117798.
<https://doi.org/10.1016/j.fuel.2020.117798>
- [39] Morrow NR, Tang G-q, Valat M, et al. Prospects of improved oil recovery related to wettability and brine composition. *Journal of Petroleum Science and Engineering* 1998;20(3):267-76.
[https://doi.org/https://doi.org/10.1016/S0920-4105\(98\)00030-8](https://doi.org/https://doi.org/10.1016/S0920-4105(98)00030-8)
- [40] Shaddel S, Tabatabae-Nejad SA, Fathi SJ. LOW-SALINITY WATER FLOODING: EVALUATING THE EFFECT OF SALINITY ON OIL AND WATER RELATIVE PERMEABILITY, WETTABILITY, AND OIL RECOVERY. 2014;5(2):133-43.
<https://doi.org/10.1615/SpecialTopicsRevPorousMedia.v5.i2.40>
- [41] Miyauchi TE, Lu Y, Firoozabadi A. Low Salinity Water Injection: Effect of Acid and Base Functionality on Recovery Performance. SPE Annual Technical Conference and Exhibition. SPE Annual Technical Conference and Exhibition. 2017.
- [42] Snosy MF, Abu El Ela M, El-Banbi A, et al. Comprehensive investigation of low salinity waterflooding in carbonate reservoirs. *Journal of Petroleum Exploration and Production Technology* 2021;12(3):701-24. <https://doi.org/10.1007/s13202-021-01330-y>
- [43] Mosallanezhad A, Kalantariasl A. Performance prediction of ion-engineered water injection (EWI) in chalk reservoirs using Response Surface Methodology (RSM). *Energy Reports* 2021;7:2916-29.
<https://doi.org/10.1016/j.egy.2021.05.012>
- [44] Ramezani M, Lashkarbolooki M, Abedini R. Experimental investigation of different characteristics of crude oil on the interfacial activity of anionic, cationic and nonionic surfactants mixtures. *Journal of Petroleum Science and Engineering* 2022;214:110485.
<https://doi.org/10.1016/j.petrol.2022.110485>
- [45] Saeed M, Jadhawar P, Ayirala SC, et al. Modelling the effects of reservoir parameters and rock mineralogy on wettability during low salinity waterflooding in sandstone reservoirs. *Journal of Petroleum Science and Engineering* 2022;215:110676.
<https://doi.org/10.1016/j.petrol.2022.110676>
- [46] Tawfik MS, Karpyn ZT, Johns RT. Effect of oil chemistry on the performance of low-salinity waterflooding in carbonates: An integrated experimental approach. *Fuel* 2022;329:125436.
<https://doi.org/https://doi.org/10.1016/j.fuel.2022.125436>
- [47] Ahmadi Aghdam M, Riahi S, Khani O. Experimental study of the effect of oil polarity on smart waterflooding in carbonate reservoirs. *Scientific Reports* 2024;14(1):22190. <https://doi.org/10.1038/s41598-024-72604-8>
- [48] Liu W, Du L, Zou X, et al. Experimental study on the enhanced ultra-heavy oil recovery using an oil-soluble viscosity reducer and CO₂ assisted steam flooding. *Geoenergy Science and Engineering* 2023;222:211409.
<https://doi.org/10.1016/j.geoen.2022.211409>
- [49] Zhang C, Jiang F, Hu T, et al. Oil occurrence state and quantity in alkaline lacustrine shale using a high-frequency NMR technique. *Marine and Petroleum Geology* 2023;154.
<https://doi.org/10.1016/j.marpetgeo.2023.106302>
- [50] He Y, Liu Y, Zhang B, et al. Low-salinity water flooding in Middle East offshore carbonate reservoirs: Adaptation to reservoir characteristics and dynamic recovery mechanisms. *Physics of Fluids* 2025;37(7).
<https://doi.org/10.1063/5.0268080>
- [51] Ma Y, Wang H, Wang W, et al. The application of Nuclear Magnetic Resonance T1-T2 maps in the research of sedimentary organic matter: A case study of early mature shale with type I kerogen. *Journal of Petroleum Science and Engineering* 2020;194:107447.
<https://doi.org/10.1016/j.petrol.2020.107447>
- [52] Liu G. Challenges and countermeasures of log evaluation in unconventional petroleum exploration and development. *Petroleum Exploration and Development* 2021;48(5):1033-47. [https://doi.org/10.1016/s1876-3804\(21\)60089-7](https://doi.org/10.1016/s1876-3804(21)60089-7)
- [53] Gmira A, Al Enezi SM, Yousef AA. Ions Dependent Stability of Stearic Acid Langmuir Monolayers: An insight of Oil/Water Interface in SmartWater Flood. SPE Middle East Oil & Gas Show and Conference. Manama, Kingdom of Bahrain: Society of Petroleum Engineers; 2017:10.
- [54] Baoukina S, Monticelli L, Risselada HJ, et al. The molecular mechanism of lipid monolayer collapse. *Proceedings of the National Academy of Sciences* 2008;105(31):10803-8.
<https://doi.org/10.1073/pnas.0711563105>

- [55] Li M, Vashaee S, Romero-Zerón L, et al. A Magnetic Resonance Study of Low Salinity Waterflooding for Enhanced Oil Recovery. *Energy & Fuels* 2017;31(10):10802-11. <https://doi.org/10.1021/acs.energyfuels.7b02166>
- [56] Trefalt G, Szilagyi I, Tellez G, et al. Colloidal stability in asymmetric electrolytes: Modifications of the Schulze–Hardy rule. *Langmuir* 2017;33(7):1695-704.
- [57] GAO X-D, LI H, TIAN R, et al. Quantitative characterization of specific ion effects using an effective charge number based on the gouy-chapman model. *Acta Physico-Chimica Sinica* 2014;30(12):2272-82.
- [58] Stachurski J, Michałek M. The effect of the ζ potential on the stability of a non-polar oil-in-water emulsion. *Journal of Colloid and Interface Science* 1996;184(2):433-6.
- [59] Collini H, Jackson MD. Zeta potential of crude oil in aqueous solution. *Advances in Colloid Interface Science* 2023:102962.
- [60] Zhou Z, Zhang C, Xi M, et al. Multi-scale modeling of natural organic matter–heavy metal cations interactions: Aggregation and stabilization mechanisms. *Water Research* 2023;238:120007.
- [61] Ikeda T, Boero M, Terakura K. Hydration properties of magnesium and calcium ions from constrained first principles molecular dynamics. *The Journal of chemical physics* 2007;127(7).
- [62] Sun Y, Han P, Hu M, et al. Insight into the salt damage mechanism to the asphalt-aggregate interface in recycled asphalt mixtures at different salt environments using molecular dynamics and DFT simulations. *Construction Building Materials* 2024;445:137931.
- [63] Oliveira Jr ON, Caseli L, Ariga K. The past and the future of Langmuir and Langmuir–Blodgett films. *Chemical reviews* 2022;122(6):6459-513.
- [64] Gu W, Li Q, Wang R, et al. Recent Progress in the Applications of Langmuir–Blodgett Film Technology. *Nanomaterials* 2024;14(12):1039.
- [65] de Ruiter R, Tjerkstra RW, Duits MH, et al. Influence of cationic composition and pH on the formation of metal stearates at oil-water interfaces. *Langmuir* 2011;27(14):8738-47. <https://doi.org/10.1021/la2010562>
- [66] Xie Q, Liu F, Chen Y, et al. Effect of electrical double layer and ion exchange on low salinity EOR in a pH controlled system. *Journal of Petroleum Science and Engineering* 2019;174:418-24. <https://doi.org/10.1016/j.petrol.2018.11.050>
- [67] Pagan Pagan NM, Zhang Z, Nguyen TV, et al. Physicochemical Characterization of Asphaltenes Using Microfluidic Analysis. *Chem Rev* 2022;122(7):7205-35. <https://doi.org/10.1021/acs.chemrev.1c00897>
- [68] Urbissinova TS, Trivedi J, Kuru E. Effect of elasticity during viscoelastic polymer flooding: a possible mechanism of increasing the sweep efficiency. *Journal of Canadian Petroleum Technology* 2010;49(12):49-56.
- [69] Haagh MEJ, Sîretanu I, Duits M, et al. Salinity-dependent contact angle alteration in oil/brine/silicate systems: the critical role of divalent cations. *Langmuir* 2017;33(14):3349-57.
- [70] Kakati A, Sangwai JS. Wettability Alteration of Mineral Surface during Low-Salinity Water Flooding: Role of Salt Type, Pure Alkanes, and Model Oils Containing Polar Components. *Energy & Fuels* 2018;32(3):3127-37. <https://doi.org/10.1021/acs.energyfuels.7b03727>
- [71] Saitua H, Gil R, Padilla AP. Experimental investigation on arsenic removal with a nanofiltration pilot plant from naturally contaminated groundwater. *Desalination* 2011;274(1-3):1-6.
- [72] Chukwudeme EA, Hamouda AA. Oil recovery from polar components (asphaltene and SA) treated chalk rocks by low salinity water and water containing SO₄²⁻ and Mg²⁺ at different temperatures. *Colloids and Surfaces A: Physicochemical and Engineering Aspects* 2009;336(1-3):174-82. <https://doi.org/10.1016/j.colsurfa.2008.11.051>
- [73] Rendel PM, Mountain B, Feilberg KL. Fluid-rock interaction during low-salinity water flooding of North Sea chalks. *Journal of Petroleum Science Engineering* 2022;214:110484.
- [74] Mokhtari R, Anabaraonye BU, Afrough A, et al. Experimental investigation of low salinity water-flooding in tight chalk oil reservoirs. *Journal of Petroleum Science Engineering* 2022;208:109282.